Kaon Electromagnetic Production on Nuclei

C. Bennhold[a], F.X. Lee[b], T. Mart[c], L.E. Wright[d]

[a]Department of Physics, George Washington University, Washington, D.C. 20052, USA

[b]Department of Physics, University of Colorado, Boulder, Colorado 80309-0446, USA

[c]Jurusan Fisika, FMIPA, Universitas Indonesia, Depok 16424, Indonesia

[d]Department of Physics, Ohio University, Athens, Ohio 45701, USA

The formation and excitation of hypernuclei through kaon photoproduction is reviewed. Basic features of the production process are emphasized. The possibility of extracting new information on hypernuclear structure and on the wave function of the bound Λ is discussed. New results are presented for the quasifree production process $A(\gamma, K\Lambda)B$. Observables of this reaction are shown to be sensitive to the Λ-nucleus final state interaction.

1. HYPERNUCLEAR EXCITATION

With the commissioning of Jefferson Lab and other continuous beam electron linacs with sufficient energy and intensity the exploration of hypernuclear structure through the electromagnetic probes is becoming a reality. In contrast to the hadronic reactions (K^-, π^-) and (π^+, K^+), the (γ, K^+) process uses rather weakly interacting probes, the photon and the K^+, with its mean free path of 5-7 fm in the nuclear medium, allowing the process to occur deep in the nuclear interior. In comparison, the K^- and the $\pi^\pm$ are both strongly absorbed, thereby confining the reaction to the nuclear periphery. Due to the mass difference in the incoming kaon and outgoing pion, the (K^-, π^-) reaction allows for recoilless Λ production in the nucleus, leading to high counting rates. Kaon photoproduction, on the other hand, involves high momentum transfers due to the large production of the rest mass which will therefore project out high momentum components of the nuclear wave functions. The subject of exciting discrete hypernuclear states through kaon photoproduction was studied extensively about 8-10 years ago[1–4] but has been mostly dormant for the last several years. However, a number of planned and approved experiments to take place within the next few years has the potential to revive interest in this field.

1.1. Matrix elements for the process $\gamma + \mathrm{A} \rightarrow K^+ +\ {}_{\Lambda}\mathrm{B}$

As shown in detail in ref.[1], the differential cross section for the reaction $\gamma + \mathrm{A} \rightarrow K^+ +\ {}_{\Lambda}\mathrm{B}$ in the center of momentum (cm) frame can be written as

$$\frac{d\sigma}{d\Omega_K^{\rm cm}} = \frac{1}{16\pi^2}\frac{q^{\rm cm}}{k^{\rm cm}}\frac{m_i m_f}{W^2}\frac{F_{\rm cm}}{2(2J_i+1)}\sum_{M_i,M_f,\lambda}|\langle J_f M_f, T_f N_f; K^+|T|J_i M_i, T_i N_i;\gamma\rangle|^2 \quad (1)$$

where we average over the initial spin projection M_i as well as the photon polarization λ and sum over the final spin projection M_f. The four-momenta of the photon and kaon are denoted by $(E_\gamma, \mathbf{k})$ and $(E_K, \mathbf{q})$, the total spin and isospin are J_i, J_f and T_i, T_f, respectively, along with their projections M_i, M_f and N_i, N_f. The usual correction factor compensating for the lack of translational invariance of the shell model is given by $F_{\rm cm} = \exp[b^2(\mathbf{k}-\mathbf{q})^2/2A]$, b being the harmonic oscillator parameter for the nucleus under study and A the nuclear mass number. The masses of the initial- and final-state nuclei are m_i and m_f, and W is the total energy in the cm system.

Taking the nuclear kaon production amplitude to be a one-body operator the nuclear matrix element is given by

$$\begin{aligned}\langle J_f M_f, T_f N_f; K^+|T|J_i M_i, T_i N_i;\gamma\rangle &= \sum_{\alpha,\alpha'}\langle J_f M_f, T_f N_f; K^+|C^\dagger_{\alpha'}C_\alpha|J_i M_i, T_i N_i;\gamma\rangle \\ &\quad\times\ \langle\alpha'; K^+|t|\alpha;\gamma\rangle\ . \end{aligned} \quad (2)$$

In Eq. (2) the many-body nuclear structure aspects are already separated from the photoproduction mechanism but in principle the sum extends over a complete set of single-particle states α and α'. The nuclear structure information involved in one-body processes is usually contained in the double-reduced density matrix elements (RDME),

$$\Psi_{J;T}(a',a) = \hat{J}^{-1}\hat{T}^{-1}\langle J_f, T_f||[C_{\alpha'}\otimes C_\alpha]||J_i, T_i\rangle\ . \quad (3)$$

All the dynamics of the photoproduction process is contained in the single-particle matrix element $\langle\alpha'; K^+|t|\alpha;\gamma\rangle$ which in general involves a nonlocal operator. In momentum space this matrix element has the form

$$\langle\alpha'; K^+|t|\alpha;\gamma\rangle = \int d^3p\ d^3q'\ \psi^*_{\alpha'}(\mathbf{p}')\phi_K^{*(-)}(\mathbf{q},\mathbf{q}')t_\gamma\psi_\alpha(\mathbf{p})\ , \quad (4)$$

where $\mathbf{p}' = \mathbf{p}+\mathbf{k}-\mathbf{q}$, and ψ is the single-particle wave function of the proton in the initial and the Λ in the final state. The wave function with the appropriate boundary conditions for the outgoing kaon of three-momentum $\mathbf{q}$, distorted by its interaction with the residual hypernucleus through an optical potential, is denoted by $\phi_K^{*(-)}(\mathbf{q},\mathbf{q}')$. This wave function is generated by solving the Klein-Gordon equation using a simple $t\rho$ optical potential with the K^+N phase shifts of ref.[6].

1.2. Basic features of the coherent kaon production process

Fig. 1 compares the momentum transfer behavior with the magnitude of the differential cross section for the reaction ${}^{16}O(\gamma, K^+)^{16}_{\Lambda}N$. At 0^o kaon lab angle the momentum transfer to the final hypernuclear system decreases as the photon lab energy increases. This leads

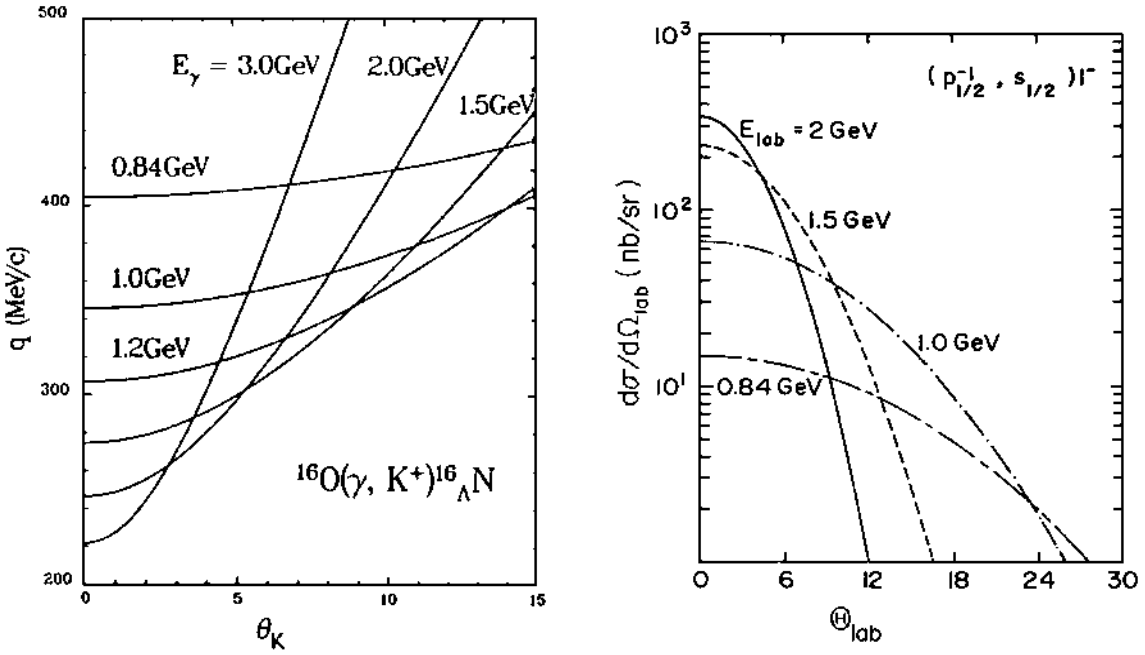

Figure 1. Kinematic features of the (γ, K^+) process. The left side shows the momentum transfer in the lab system for several photon energies E_γ. The right side shows angular distributions for the 1^- member of the ground state doublet in $^{16}O(\gamma, K^+)^{16}_{\Lambda}N$ for various photon lab energies.

to a differential cross section at $\Theta_K = 0^o$ which increases as E_γ increases, from around 15 nb/sr at 0.84 GeV to 330 nb/sr at 2 GeV for the particular transition shown. However, the momentum transfer increases more rapidly for non-zero kaon angles at higher photon energies. Thus, the angular distributions become more forward peaked and fall off more rapidly. The energy chosen for an experiment therefore depends on the desired result: if the goal is to perform hypernuclear spectroscopy choosing a higher photon energy around 2 GeV, while detecting the K^+ under 0^o would be advantageous. If, on the other hand, one likes to extract dynamical information by mapping our transition densities via measuring angular distributions, photon energies of 1.0 to 1.2 GeV would be preferable.

With the exception of ref.[3,5] all calculations up to now have been performed in pure particle-hole configurations. These predictions may be reliable where the proton pick-up strength is not highly fragmented for stretched spin-flip transitions with maximum $J = l_N + l_\Lambda + 1$. These transitions are usually dominated by the Kroll-Ruderman $\boldsymbol{\sigma} \cdot \boldsymbol{\epsilon}$ operator and tend to have the largest cross sections. In the case shown in Fig. 1 we describe $^{16}_{\Lambda}N$ as a pure $p_{1/2}$ proton hole coupled to an s-shell Λ, coupling to a 0^- and 1^- ground state transition. The degeneracy between these two states would be removed by including the ΛN interaction. For a closed shell target nucleus in a pure particle-hole basis, the RDME simply reduce to $\Psi_{J;T}(a', a) = \delta_{ab}\delta_{a'b'}$. While the stretched transitions are most likely the first ones to be measured, eventually one would like to use the (γ, K^+)

reaction to extract hypernuclear structure information from cases where configuration mixing is important. As discussed in ref.[7], the reaction ${}^9Be(\gamma, K^+)^9_\Lambda Li$ may provide a good testing ground for resolving members of the s_Λ doublet of $3/2^+$ and $5/2^+$, coupling the s-shell Λ to the 2^+ core of ${}^8Li$. This doublet is split by 0.51 MeV according to the "standard" ΛN interaction of ref.[8]. The predicted $\Delta S = 0$ RDME are large for the lower member of the doublet but small for the upper member while there is a large $\Delta J = 2$ ($\Delta S = 1$) RDME for the upper member; thus, the two transitions would produce very different angular distributions. Similar information may be extracted from the reaction ${}^{13}C(\gamma, K^+)^{13}_\Lambda B$.

1.3. The role of the elementary operator

Over the last several years considerable effort has been spent to develop models for the electromagnetic production of kaons from nucleons at photon energies below 2 GeV[9–12]. Most of these analyses have focused on the two processes $\gamma p \to K^+\Lambda$ and $\gamma p \to K^+\Sigma^0$, using real or virtual photons, since almost all of the few available photokaon data have been taken for these two reactions. Due to the limited set of data the various models permit only qualitative conclusions but do not yet allow the extraction of precise coupling constants and resonance parameters.

Fig. 2 illustrates the sensitivity of the hypernuclear formation cross sections to different elementary amplitudes for the stretched 3^+ excited state and the 0^- ground state transition. All the amplitudes used give an equally good fit to the available cross section data on the nucleon. The results for the 3^+ state are similar in shape and differ by at most 50% in magnitude while different operators can lead to angular distributions differing by more than an order of magnitude. This can be traced to the dominance of the Kroll-Ruderman term in the 3^+ transition which is shown to deviate from the full operator only slightly in the right panel of Fig. 2. The 0^- state, on the other hand, is clearly very sensitive to details of the non spin-flip pieces of the operator. Retaining the $\boldsymbol{\sigma} \cdot \boldsymbol{\epsilon}$ term only overestimates the cross section by more than an order of magnitude and misses the minimum from the form factor. Clearly, the elementary process has to be measured more precisely before reliable predictions can be made.

The stretched transitions such as the 3^+ state discussed above can be used to extract the bound Λ wave function. If a transition is dominated by the Kroll-Ruderman term, the operator becomes local and can be factored out of the single-particle matrix element of Eq. 4. Furthermore, neglecting kaon distortion which reduces cross sections only by about 10-20% for p-shell nuclei reduces the matrix element to

$$\langle \alpha'; K^+|t|\alpha;\gamma\rangle \;\; = \;\; const. \int r^2 dr \; \psi^*_\Lambda(r)\psi_p(r) j_L(Qr) \; . \tag{5}$$

Therefore, assuming one has good knowledge of the bound proton wave function from $(e, e'p)$, measuring an angular distribution will map out the bound Λ wave function. This feature is unique to the (γ, K^+) process since distortion effects are minimal.

2. EXCLUSIVE QUASIFREE KAON PHOTOPRODUCTION

Due to the sizable momentum transfer to the hypernuclear system the probability of forming such bound states is in fact rather small. Ref.[2] has estimated this formation

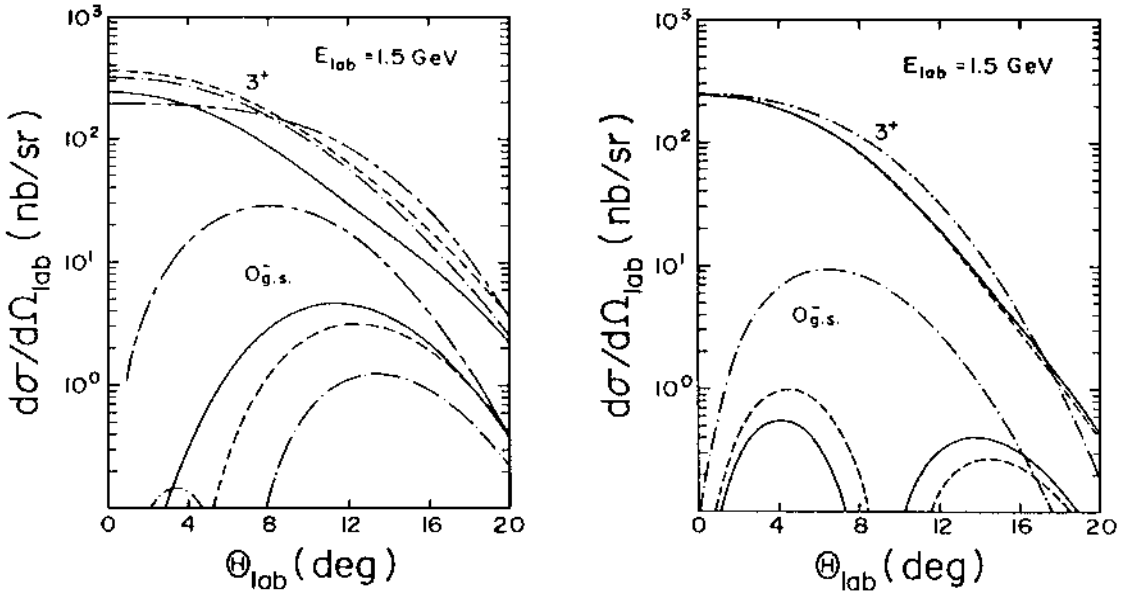

Figure 2. Sensitivity of the hypernuclear cross section to the elementary operator. The left side compares angular distributions for $^{16}O(\gamma, K^+)^{16}_{\Lambda}N$ using different elementary amplitudes (see ref.[1] for details), while the right side compares the full operator (dashed curve) to the nonrelativistic reduction (solid curve) and the $\boldsymbol{\sigma} \cdot \boldsymbol{\epsilon}$ term only (dash-dotted curve).

probability to be around 5-10% of the total (γ, K^+) strength on nuclear targets, thus most of the kaon production events will come from quasifree production. Here we present the first theoretical predictions for quasifree kaon photoproduction from nuclei, $A(\gamma, KY)B$, where the kaon can be a K^+ or K^0, and the hyperon can be either a Λ or a Σ. Thus, if this process is measured exclusively six possible reaction channels can be explored. The predictions are made in a DWIA framework that has been successfully applied in our previous work on quasifree pion photo- and electroproduction[13] and eta photoproduction on nuclei[14]. This reaction allows for the study of the reaction process in the nuclear medium as well as final state interaction effects without being obscured by the details of the nuclear transitions as discussed above. This is due mainly to the quasifree nature of the reaction which permits the kinematic flexibility to have small momentum transfers. The key ingredients are: a) the single-particle wave function and spectroscopic factor, usually taken from electron scattering, b) the elementary kaon photoproduction amplitude, obtained from measuring the the free processes, c) the distorted kaon wave function which can be taken from kaon elastic scattering in case of the K^+, and finally, d) the hyperon-nucleus final-state interaction. It is mainly to study the last ingredient that we investigate this process which is already part of an approved TJNAF experiment in Hall B.

2.1. Matrix elements and observables

The coordinate system is defined such that the z-axis is along the photon direction $\mathbf{k}$, and the y-axis is along $\hat{\mathbf{k}} \times \hat{\mathbf{q}}$ with the azimuthal angle of the kaon chosen as $\phi_K = 0$. The kinematics of the reaction are determined by $\mathbf{k} = \mathbf{q} + \mathbf{p} + \mathbf{Q}$ and $E_\gamma + M_i = E_K + E_Y + M_f + T_Q$. Here $\mathbf{Q}$ and $T_Q = \frac{Q^2}{2M_f}$ are the missing momentum and missing kinetic energy in the reaction, respectively, and $|\mathbf{k}| = E_\gamma$ for real photons. The binding energies are included in the masses M_i and M_f. In the impulse approximation, the reaction is assumed to take place on a single bound nucleon whose energy and momentum are given by $\mathbf{p}_i = -\mathbf{Q}$ and $E_i = E_K + E_Y - E_\gamma$. The struck nucleon is in general off its mass shell.

In contrast to hypernuclear production discussed above, the reaction is *quasifree*, meaning that the magnitude of $\mathbf{Q}$ has a wide range, including zero. Since the reaction amplitude is proportional to the Fourier transform of the bound state single particle wavefunction, it falls off quickly as the momentum transfer increases. Thus, we will restrict ourselves to the low Q region (< 500 MeV/c) where the nuclear recoil effects can be safely neglected for nuclei of $A > 6$.

The differential cross section can be written as

$$\frac{d^3\sigma}{dE_K\, d\Omega_K\, d\Omega_Y} = \frac{C}{2(2J_i+1)} \sum_{\alpha,\lambda,m_s} \frac{S_\alpha}{2(2j+1)} |T(\alpha,\lambda,m_s)|^2, \tag{6}$$

where the kinematical factor is given by

$$C = \frac{M_f m_Y\, |\mathbf{q}|\, |\mathbf{p}|}{4(2\pi)^5 |E_Y + M_f + T_Q - E_Y\, \mathbf{p}\cdot(\mathbf{k}-\mathbf{q})/p^2|}. \tag{7}$$

The single particle matrix element is given by

$$T(\alpha,\lambda,m_s) = \int d^3r\, \Psi^{(+)}_{m_s}(\mathbf{r},-\mathbf{p})\, \phi^{(+)}_K(\mathbf{r},-\mathbf{q})\, t_{\gamma K}(\lambda,\mathbf{k},\mathbf{p}_i,\mathbf{q},\mathbf{p})\, \Psi_\alpha(\mathbf{r})\, e^{i\mathbf{k}\cdot\mathbf{r}}. \tag{8}$$

In the above equations, J_i is the target spin, $\alpha = \{nljm\}$ represents the single particle states, S_α is called the spectroscopic factor whose value is taken from electron scattering, λ is the photon polarization, m_s is the spin projection of the outgoing nucleon, $\Psi^{(+)}_{m_s}$ and $\phi^{(+)}_K$ are the distorted wavefunctions with outgoing boundary conditions, Ψ_α is the bound nucleon wavefunction, and $t_{\gamma K}$ is the kaon photoproduction one-body operator.

We also compute the photon asymmetry, defined by

$$\Sigma = \frac{d^3\sigma_\perp - d^3\sigma_\parallel}{d^3\sigma_\perp + d^3\sigma_\parallel} \tag{9}$$

where $\perp$ and $\parallel$ denote the perpendicular and parallel photon polarizations relative to the production plane (x-z plane), and the hyperon recoil polarization (also referred to as analyzing power) defined by

$$P = \frac{d^3\sigma_\uparrow - d^3\sigma_\downarrow}{d^3\sigma_\uparrow + d^3\sigma_\downarrow} \tag{10}$$

where $\uparrow$ and $\downarrow$ denote the polarizations of the outgoing hyperon relative to the y-axis. We have used the short-hand notation $d^3\sigma \equiv d^3\sigma/dE_K\, d\Omega_K d\Omega_Y$ with appropriate sums

over spin labels implied. Note that P is obtained for free since the produced hyperon is self-analyzing, while the measurement of Σ requires a linearly polarized photon beam.

For the bound nucleon, we use harmonic oscillator wavefunctions which are sufficient in the quasifree region we are interested in. For the outgoing kaon the same distorted wave function is used as in hypernuclear production discussed above.

2.2. The hyperon-nucleus optical potentials

Very few optical potentials have been constructed for the Λ and Σ, mostly due to lack of data. Here, we employ the global optical model of ref.[15]. It is based on a global nucleon-nucleus Dirac optical potential fit[16]. The parameters of the potential are motivated by the constituent quark model and adjusted to fit the hypernuclear binding energy data We use its nonrelativistic equivalent version which has a central part and a spin-orbit part: $U(r) = U_{cen}(r) + U_{so}(r)\ \sigma \cdot \mathbf{l}$. Note that the spin-orbit part is multiplied by a factor that depends on the partial wave under consideration. Fig. 3 shows the real and imaginary parts of both $U_{cen}(r)$ and $U_{so}(r)$ on ^{12}C at 200 MeV kinetic energy for the Λ and the Σ^0. For comparison, they are also shown for proton. The real parts of the central potential are clearly smaller than the proton potential by around a factor of two, reflecting the fact that Lambdas have a smaller binding energy in hypernuclei while Sigmas appear not to be bound at all. The imaginary part of the Σ's central potential is similar in magnitude to that of the nucleon, due to the large $\Sigma N \rightarrow \Lambda N$ conversion width. The very small spin-orbit potential of the Λ is a reflection of the ΛN spin-orbit force which is known to be small.

2.3. Results and discussion

Our results are shown in Fig. 4 for the reaction $^{12}C(\gamma, KY)^{11}B_{g.s.}$ at E_γ=1.4 GeV and Q=120 MeV/c under quasifree kinematics. Quasifree kinematics is similar to two-body kinematics in free space, except that the nucleon is bound with finite momentum Q.

As the kaon angle increases, the kaon energy decreases, the hyperon energy increases, the hyperon angle increases to a certain value, then decreases. In this particular case, the kaon and hyperon energies reach around 500 to 700 MeV, and the hyperon angle reaches up to 45 degrees, depending on the channel. Fig. 4 shows the differential cross sections as well as two polarization observables, comparing PWIA calculations with results that include hyperon and kaon final state interaction (FSI). As in the case of hypernuclear production discussed above kaon distortion reduces the cross sections by about 10-20% but has little effect on the polarization observables. In the case of $K^0\Sigma^0$ production we have used the same optical potential as for the K^+ since little is known about the K^0 nucleus interaction. In principle, such information can be obtained by measuring kaon charge exchange on nuclei. Including the hyperon FSI reduces the angular distributions by up to 30% at forward angles. Again, with the exception of the recoil polarization in $K^+\Lambda$ production, the polarization observables are barely affected by the inclusion of FSI. This situation is similar to our previous findings in quasifree pion and eta photoproduction[13,14]. It opens the possibility to use the polarization observables as a way to study modifications of the basic production process in the nuclear medium. The magnitudes of the Σ and P observables is sizeable and should be measurable. However, they are very sensitive to the elementary operator used, thus, given our limited knowledge of the elementary process, the polarization observables shown here should be treated with caution. The first set of

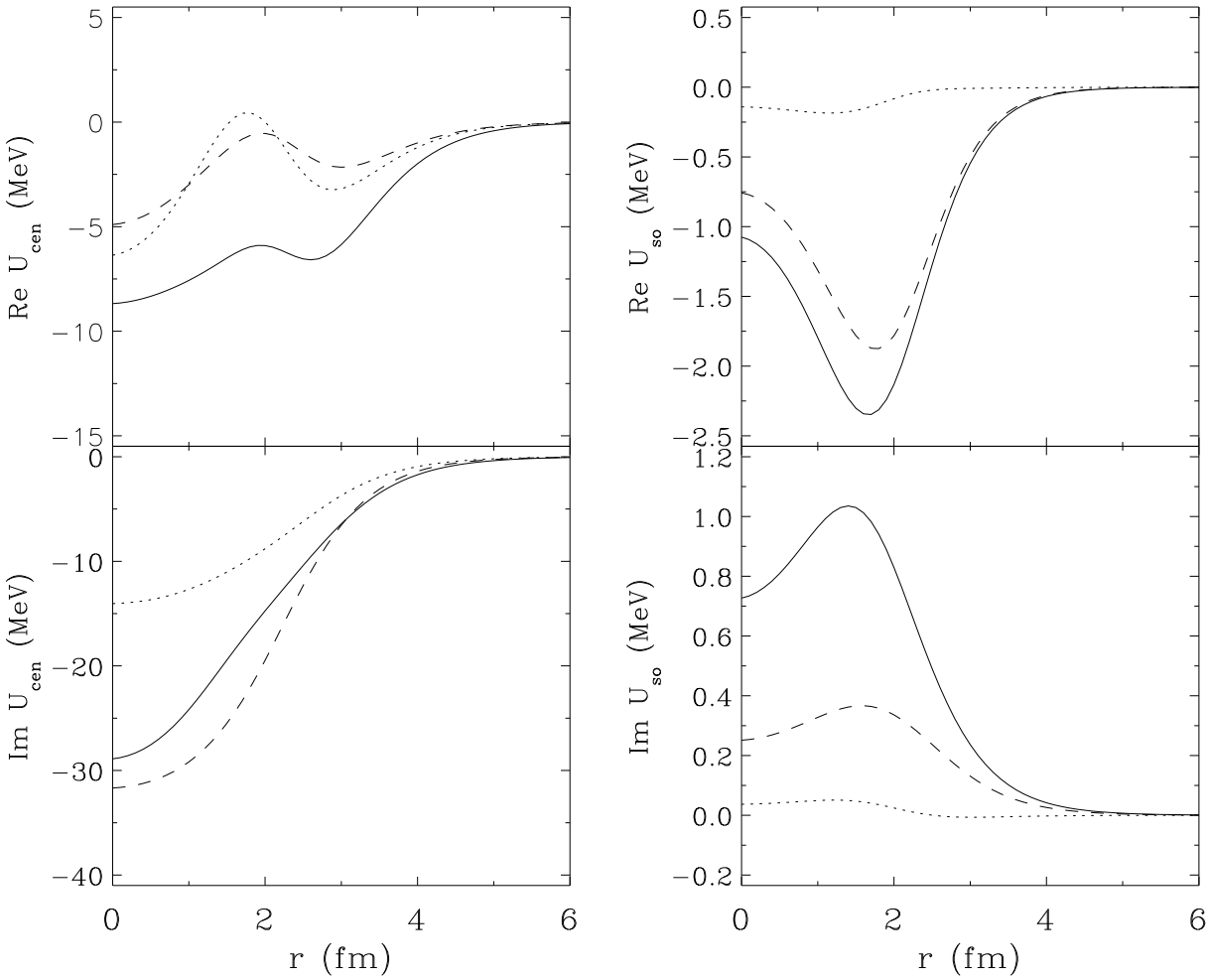

Figure 3. Hyperon optical potentials for ^{12}C at 200 MeV kinetic energy. The dashed line shows the Λ potential, while the dotted line depicts the Σ^0 potential. The proton potential (solid line) is shown for comparison.

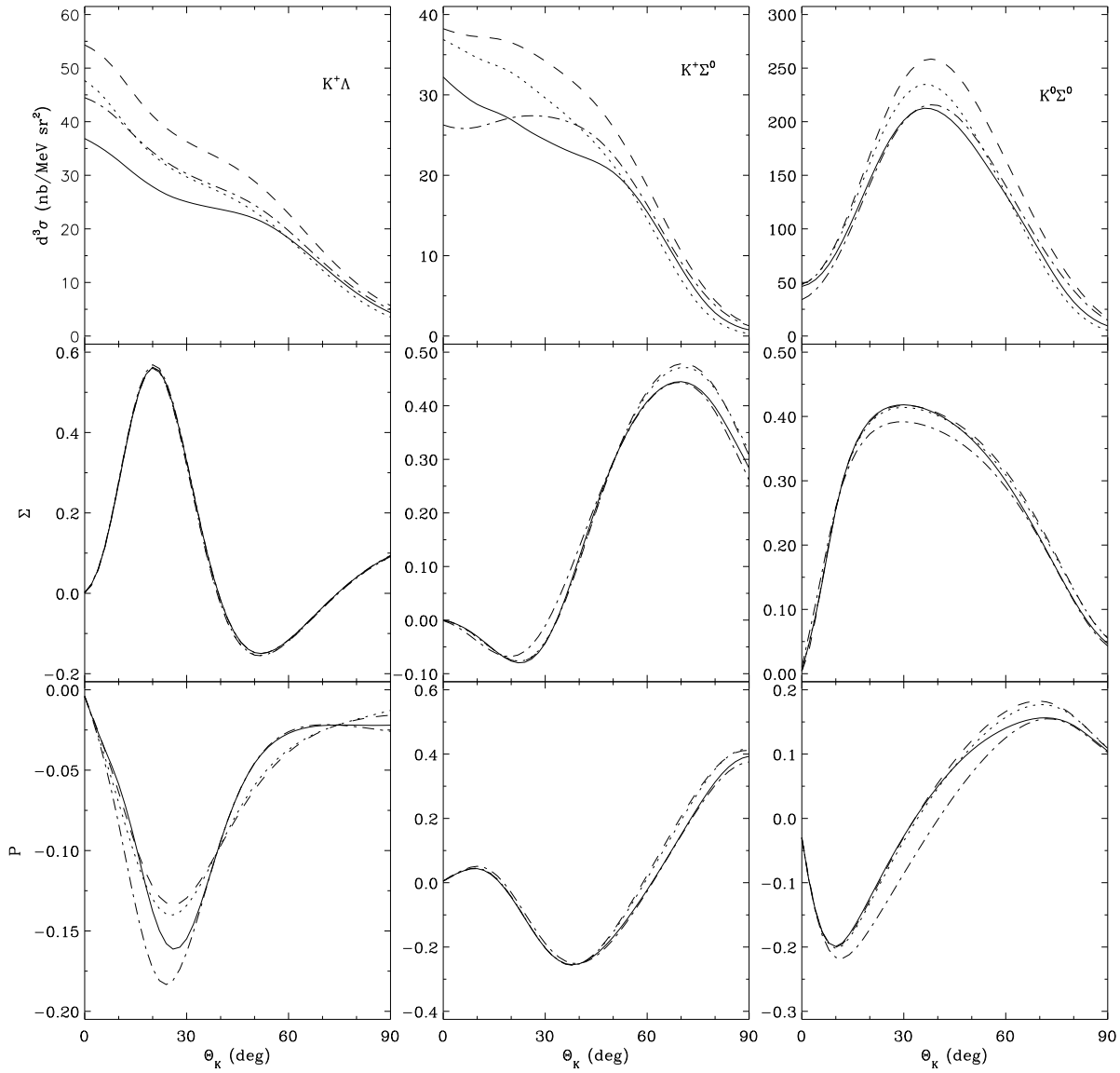

Figure 4. Results for the reaction $^{12}C(\gamma, KY)B_{g.s.}$ at E_γ=1.4 GeV and Q=120 MeV/c under quasifree kinematics. Three of the six possible channels are shown in the three columns, using the model of Ref. [11] for the elementary process. The four curves correspond to calculations in PWIA (dashed), in DWIA with kaon only distorted (dotted), with hyperon only distorted (dash-dotted), and with both distorted (solid).

CLAS experiments with new data for the kaon production reactions on the nucleon will allow a precise determination of the elementary amplitude which in turn can be used to reliably predict these observables.

REFERENCES

1. C. Bennhold and L.E. Wright, Phys. Rev. C39 (1989) 927; Phys. Lett. 191B (1987) 11; Prog. Part. Nucl. Phys. 20 (1988) 377.
2. S.R. Cotanch and S.S. Hsiao, Nucl. Phys. A 450 (1986) 419c.
3. A.S. Rosenthal *et al.*, Ann. Phys. (NY) 184 (1988) 33; A.S. Rosenthal, D. Halderson, and F. Tabakin, Phys. Lett. B 182 (1986) 143.
4. J. Cohen, Phys. Rev. C 32 (1985) 543; Intern. J. of Mod. Phys. A4 (1989) 1.
5. T. Motoba, M. Sotona, and K. Itonaga, Prog. Theor. Phys. Suppl. 117 (1994) 123.
6. B.R. Martin, Nucl. Phys. B94 (1975) 413.
7. C.B. Dover and D.J. Millener, in Modern Topics in Electron Scattering (World Scientific, Singapore, 1990, B. Frois and I. Sick, eds.)
8. D.J. Millener et al., Phys. Rev. C31 (1985) 499.
9. R.A. Adelseck, C. Bennhold, and L.E. Wright, Phys. Rev. C 32 (1985) 1681; H. Tanabe, M. Kohno, and C. Bennhold, Phys. Rev. C 39 (1989) 741.
10. J.C. David, C. Fayard, G.H. Lamot, and B. Saghai, Phys. Rev. C 53 (1996) 2613.
11. R.A. Williams, C.-R. Ji, and S.R. Cotanch, Phys. Rev. C46 (1992) 1617.
12. T. Mart, C. Bennhold, and C. E. Hyde-Wright, Phys. Rev. C51 (1995) R1074; T. Mart and C. Bennhold, Few-Body Sys. Suppl. 9 (1995) 369.
13. X. Li (F.X. Lee), L.E. Wright, and C. Bennhold, Phys. Rev. C 48 (1993) 816; Phys. Rev. C 50 (1994) 1283.
14. F.X. Lee, L.E. Wright, C. Bennhold, L. Tiator, Nucl. Phys. A 603 (1996) 345.
15. E.D. Cooper, B.K. Jennings and J. Mareš, Nucl. Phys. A580 (1994) 419; Nucl. Phys. A585 (1995) 157.
16. E.D. Cooper, S. Hama, B.C. Clark, and R.L. Mercer, Phys. Rev. C47 (1993) 297.